*Proceedings of **BITCON-2015** Innovations For National Development*
National Conference on : Innovations In Mechanical Engineering For Sustainable Development

Research Paper

CFD ANALYSIS OF NOZZLE IN ABRASIVE WATER SUSPENSION JET MACHINING

Saurabh Verma[1], S. K. Mishra[2] and S.K. Moulick[3]

Address for Correspondence

[1]Student of production engineering, [2]Assistant Professor, [3]Professor of Mechanical engineering,
Bhilai Institute of Technology, Durg (CG) India

ABSTRACT

Abrasive water suspension jet (AWSJ) machining process utilized increasingly in industrial applications. It is a non-traditional machining process and involves complex mechanics. A nozzle is required to perform abrasive water suspension jet machining for material removal with the help of very high velocity of water suspension jet. The main problem of AWSJ machining process is nozzle wear during the process. The wear depends on various parameters such as water jet characteristics, abrasive size and nozzle geometry, etc. The nozzle wear is not fully understood experimentally; also the uncontrolled nozzle wear can affect the effectiveness and surface finish obtained through the AWSJ machining process. In the present work, the effect of geometrical parameters of single step nozzle and abrasive size on skin friction coefficient at the wall of nozzle due to wall shear stress and jet exit kinetic energy has been analyzed by ANSYS software. This analysis is totally depends on nozzle geometry and nozzle material is taken same for all cases. This analysis can be highly helpful for understanding nozzle wear during the AWSJ machining process.

KEY WORDS: Abrasive water suspension jet (AWSJ) machining, nozzle geometry, nozzle wear, fluid flow, MRR, Erosion rate.

1. INTRODUCTION

Abrasive water suspension jet (AWSJ) machining process is non-conventional machining process, which has been used in industrial applications. AWSJ machining process operates at relatively high-pressure (10-1000 M Pa) and focused stream of abrasive particles carried by high pressure water is made to impinge on the work material is removed by erosion by high velocity Abrasive particles. In abrasive water suspension jet machining process pure water (tap water) is used and for abrasive particles like sand (SiO_2), glass beads, Aluminum oxide, and silicon carbide is generally used. In AWSJ machining in which suspended abrasive particles in liquid medium called slurry is pressurized and expelled through the nozzle. Slurry is accelerated through a fine orifice to produce a high velocity stream, which is capable of machining a range of materials. Two types of nozzles generally used for average material removal, tungsten carbide nozzle have a useful life of 12 to 13 hr. and sapphire nozzles have a useful life of 3hr. Benefit of AWSJ over AWJ is the generation of stable jet with higher power density, which leads to efficient energy transfer to abrasive particles. Nozzle wear is a complex phenomenon, which is not only influenced by the material properties of the nozzle but also by the nozzle geometry and operating parameters of AWSJ.M. Hashish et al [2] have done experimental investigation that observation of wear of abrasive water jet nozzle materials. Hardness and toughness of nozzle material influence of nozzle wear. M. Nanduri et al [6] has investigated experimentally the effect of nozzle geometric parameters and system parameters on nozzle wear was studied. An empirical model was developed for the prediction the wear.A Beautiful attempt to decrease the nozzle wears in AWSJ cutting. Umang anand et al [8] has done experimental investigation that, the used porous nozzle surrounded by a reservoir containing high viscosity lubricant and concluded that type of nozzle used for preventing nozzle wear in AWSJ cutting.

Jegaraj J et al [10] has done experimental work and gave strategy for the efficient and quality cutting of materials and suggest that to achieve higher efficiency and desired quality, it is required to monitor the condition of nozzles and considering the change in the dimension of orifice and focusing nozzle. Kyriaki et al [11] has done software analysis on AWJ machining analyzed in detail the work piece material behavior under water jet impingement, a non-linear FE model (using LS-DYNA 3D code) was developed for studying the water jet cutting process and it can be used for the optimization of the water jet parameters. Mostofa et al [17] CFD and theoretical analysis of abrasive water jet cutting head the simulation results show that the velocity of the water jet contribute the erosion rate at the nozzle wall, and erosion rate increases on the focusing tube wall with the change in the particle shape factor. Deepak et al [20] CFD investigation that how effect of inlet operating pressure on skin friction coefficient and jet exit kinetic energy in single step nozzle in AWSJ machining.

2. THEORETICAL FORMULATION

2.1. Numerical Model and Assumptions

The numerical region for flow analysis is made up of flow geometry given in the Fig. 1 for the single step AWSJ nozzle. Computational domain consists of converging nozzle of diameter 4mm, nozzle length 4mm straight duct is introduced. There is a focus tube of diameter 1.3mm and length 17mm. The Abrasive water suspension mixture is let into the nozzle at the inlet and is carried down through the converging cone to the focus tube and exits as coherent jet at the nozzle exit, in which the focus tube is used for stabilizing the flow.

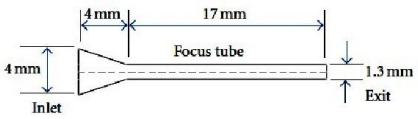

Fig.1: Computational domain of single step nozzle according to Deepak et al [20].

The numerical model adopted closely follows the work of G.Hu et al [14] in which liquid solid two-phase flow is considered and the following assumptions are valid for the present work.

I. The primary liquid phase is continuous and incompressible.

II. Flow is taken to be two-phase flow in which the primary liquid phase mixes homogeneously with the particles of equal diameter, constituting the solid phase.

III. Two-phase flow assumed is steady and characterized by turbulent flow.

2.2 The computation of particulate loading and stokes number

Particulate loading and the stokes number are important parameters that help to identify the appropriate multiphase model. Particulate loading has a major impact on phase interactions and is defined as the mass density ratio of the dispersed phase to that of the carrier phase.

The particulate loading for garnet abrasive is

$$\beta = \frac{\alpha_s \rho_s}{\alpha_l \rho_l} = \frac{0.1x2300}{998} = 0.230 \quad (1)$$

For silicon carbide abrasive is

$$\beta = \frac{\alpha_s \rho_s}{\alpha_l \rho_l} = \frac{0.1x3170}{998} = 0.318 \quad (2)$$

For aluminum oxide abrasive is

$$\beta = \frac{\alpha_s \rho_s}{\alpha_l \rho_l} = \frac{0.1x2719}{998} = 0.27 \quad (3)$$

The degree of interaction between the phases is intermediate loading, the coupling is two-way i.e., the fluid carrier influences the particulate phase via drag and turbulence, but the particles in turn influence the carrier fluid via reduction in mean momentum and turbulence. All multiphase models can handle this type of problem but it is found that the Eulerian multiphase model seems to be the most accurate one. The average distance between the individual particles of the particulate phase can be estimated by equation developed by Crowe et al (2009).

For garnet abrasive:

$$\gamma = \frac{\rho_s}{\rho_l} = \frac{2300}{998} = 2.3 \quad (4)$$

$$k = \frac{\beta}{\gamma} = \frac{0.230}{2.30} = 0.100 \quad (5)$$

$$\frac{L}{d_p} = \left(\frac{\pi}{6}\frac{1+k}{k}\right)^{\frac{1}{3}} = \left(\frac{\pi}{6}\frac{1+0.10}{0.10}\right)^{\frac{1}{3}} = 1.7925 \quad (6)$$

The average distance between the individual particles (particle size d_p=63µm) of the particulate phase is

$$L = 1.7925 \times d_p = 1.7925 \times 0.063 = 0.1129\text{mm}$$

Estimating the value of the stokes number helps to select the most appropriate multiphase model. The stokes number is defined as the ratio of the particleresponse time to the system response time is calculated below.

$$\tau_d = \frac{\rho_d d_d^2}{18\mu_l} = \frac{2300x(63x10^{-6})^2}{18x0.001004} = 5.05123x10^{-4} \quad (7)$$

$$t_s = \frac{l}{v} = \frac{0.0364}{25.6} = 1.4218x10^{-3} \quad (8)$$

$$S_t = \frac{\tau_d}{t_s} = \frac{5.05129x10^{-4}}{1.4218x10^{-3}} = 0.3552 \quad (9)$$

For silicon carbide abrasive:

$$\gamma = \frac{\rho_s}{\rho_l} = \frac{3170}{998} = 3.18 \quad (10)$$

$$k = \frac{\beta}{\gamma} = \frac{0.318}{3.18} = 0.1 \quad (11)$$

L = 1.7925×0.063 = 0.1129mm

$$\tau_d = \frac{\rho_d d_d^2}{18\mu_l} = \frac{3170x(63x10^{-6})^2}{18x0.001004} = 6.96200x10^{-4} \quad (12)$$

$$t_s = \frac{l}{v} = \frac{0.0364}{25.6} = 1.4218x10^{-3} \quad (13)$$

$$S_t = \frac{\tau_d}{t_s} = \frac{5.05129x10^{-4}}{1.4218x10^{-3}} = 0.3551 \quad (14)$$

For Aluminum oxide abrasive:

$$\gamma = \frac{\rho_s}{\rho_l} = \frac{2719}{998} = 2.72 \quad (15)$$

$$k = \frac{\beta}{\gamma} = \frac{0.272}{2.72} = 0.1 \quad (16)$$

$$\frac{L}{d_p} = \left(\frac{\pi}{6}\frac{1+k}{k}\right)^{\frac{1}{3}} = \left(\frac{\pi}{6}\frac{1+0.1}{0.1}\right)^{\frac{1}{3}} = 1.7925 \quad (17)$$

L = 1.7925×0.063 = 0.1129mm

$$\tau_d = \frac{\rho_d d_d^2}{18\mu_l} = \frac{2719x(63x10^{-6})^2}{18x0.001004} = 5.97151x10^{-4} \quad (18)$$

$$t_s = \frac{l}{v} = \frac{0.0364}{25.6} = 1.4218x10^{-3} \quad (19)$$

$$S_t = \frac{\tau_d}{t_s} = \frac{5.05129x10^{-4}}{1.4218x10^{-3}} = 0.3552 \quad (20)$$

For Stokes number less than unity, particles will closely follow the fluid flow and any one of the three multiphase models namely Volume of fluid model, Mixture model or Eulerian multiphase model is applicable. Also from the calculation of the effect of particulate loading it is clear that coupling between two phases is intermediate. Hence present numerical simulation is carried using Eulerian multiphase model which through is most expensive in computation, but gives most accurate results. Eulerian Multiphase model is embedded in fluent software. Fluent solves a multi-fluid granular model to describe the flow behavior of fluid solid mixture. The stresses induced in the solid phase are deduced through an analogy between the random particle motion arising from particle to particle collisions and the thermal gradient of molecules in the fluid stream taking into effect the inelasticity of the granular phase. Intensity of the particle velocity fluctuations determines the stresses, viscosity and pressure of the solid phase.

The governing equations for mass and momentum conservation are solved for the steady incompressible flow. The coupling between velocity and pressure has been attempted through the phase couples SIMPLE algorithm developed by Patankar S.V. using the power law scheme for the solution. The turbulence is modeled using Realizable k-€ turbulence model. The governing partial differential equations, for mass and momentum conservations are detailed below.

Continuity Equation:

$$\frac{1}{\rho_{pq}}\left[\frac{\partial}{\partial t}(\alpha_q \rho_q) + \nabla\cdot(\alpha_q \rho_q v_q)\right] = \sum_{p=1}^{N}(m_{pq} - m_{qp}) \quad (21)$$

Where

p,q phases, α_q= vol.fraction of the secondary phase, ρ_{pq}= density of suspended mixture(kg/m^3), v= velocity, m= mass flow rate, N= lift force

Fluid-solid Momentum Equation:

The conservation of momentum equation for the solid phase is as follows:

$$\frac{\partial}{\partial t}(\alpha_s \rho_s v_s) + \nabla(\alpha_s \rho_s v_s^2) = -\alpha_s \nabla p - \nabla p_s + \nabla\cdot\tau_s + \alpha_s \rho_s g + \sum_{l=1}^{N}[k_{ls}(v_l - v_s) + (m_{ls} v_{ls} - m_{sl} v_{sl})] + (F_s + F_{lift,s} + F_{vm,s}) \quad (22)$$

Where α_s=vol. fraction of solid phase, ρ_s= density of the solid phase, v_s=velocity of the solid phase, τ_s= particle response time, l= length of flow domain (mm), F_s=external body force, $F_{vm,s}$=virtual mass force of solid phase, F_{lift}= lift force of solid phase, m = mass flow rate, K= momentum exchange coefficient

The conservation of momentum equation for the fluid phase is as follows.

$$\frac{\partial}{\partial t}\left(\alpha_q \rho_q v_q\right) + \nabla\left(\alpha_q \rho_q v_q^2\right) = -\alpha_q \nabla p + \nabla \cdot \tau_q + \alpha_q \rho_q g + \sum_{l=1}^{N}\left[k_{pq}\left(v_p - v_q\right) + \left(m_{pq} v_{pq} - m_{qp} v_{qp}\right)\right] + \left(F_q + F_{lift,q} + F_{vm,q}\right) \quad (23)$$

2.3 Particle Erosion and Accretion Theory

Particle erosion and accretion rates can be monitored at wall boundaries. The erosion rate is defined as [5]:

$$R_{erosion} = \sum_{p=1}^{N_{particle}} \dot{m}_p \frac{c(d_p) f(\alpha) v^{b(v)}}{A_{face}} \quad (24)$$

Where

c(dp) = function of particle diameter
α = impact angle of the particle path with the wall face
f (α) = function of impact angle
v = relative particle velocity
b(v) = function of relative velocity
A_{face} = Area of the cell face at the wall
Defaults values are c = 1.8×10-9, f = 1 and b = 0.

3. METHOD OF SOLUTION

3.1. Numerical Scheme

Conservation equations are solved for each control volume to obtain the velocity and pressure fields. Convergence is affected when all the dependent variable residuals fall below 0.00001 at all grid points. Computational domain is modeled using commercially available pre-processor routine called GAMBIT and meshing is carried out using appropriate grid cells of suitable size available in the software routine. Wall region in the flow domain is closely meshed using the boundary layer mesh concepts for extracting high velocity gradients near the boundary walls. According to the structure of nozzle jet characteristics, computational domain is built as axi-symmetric model. Fig.3 and Fig. 4 shows the computational domain. According to Deepak et al [20]. Grid independence test is performed to check the quality of mesh for solution convergence as shown in Fig.2 it is clear from the grid independence study that found that there is almost negligible variation (not more than 1%), in the axial velocity distribution for the between mesh geometries of 21200, 25440 and 29690 control volumes. Hence considering for a higher quality of solution a mesh geometry consisting of 30000 control volumes has been adopted in this work.

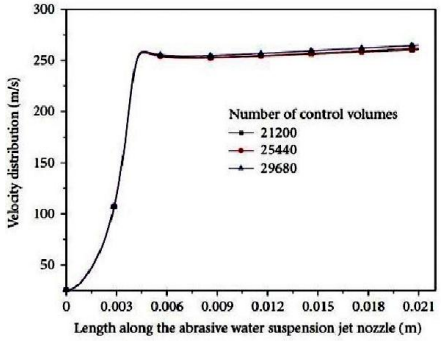

Fig. 2 Result of grid independence test for the AWSJ nozzle [20].

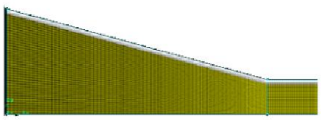

Fig. 3 A portion of meshed domain near the critical section of AWSJ nozzle.

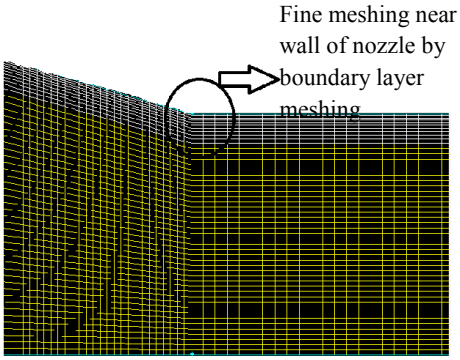

Fig. 4 A meshed domains near the wall of nozzle

3.2 Boundary Condition and Operating Parameters

Suitable boundary conditions are imposed on the computational domain, as per the physics of the problem. Inlet boundary condition is specified by the operating pressure entering the nozzle. It is assumed that velocity at inlet is uniform across the cross section. At the exit, static pressure of refluxing flow is taken to be zero (gauge), so that the computation would proceed by the relative pressure difference across the grid volumes for the entire domain of the flow. Wall boundary conditions are impressed to bound fluid and solid regions. In viscous flow models, as in the present case velocity components at the wall are set to zero in according with the no-slip and impermeability conditions that exist on the wall boundary. The axis of the nozzle is used to solve the computational domain as axis-symmetric problem and suitable boundary conditions are imposed for the same i.e., the gradient of fluid properties are set to zero across the axis line. In the present numerical simulation suspended liquid is treated as primary phase and abrasive is treated as secondary phase.

4. RESULTS AND DISCUSSION

4.1. Validation of the Numerical Model

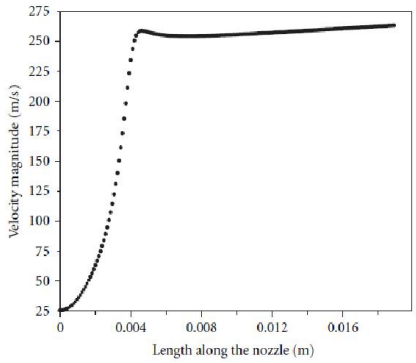

Fig. 5: The velocity distribution along the length of the single step nozzle as given in reference literature [20].

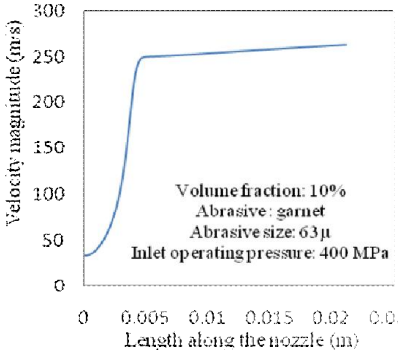

Fig. 6: The velocity distribution along the length of the single step nozzle as per the present model.

The present model is benchmarked against the numerical work according to Deepak et al. (2012) cited in [20]. The graph of the velocity distribution of one of the phases (liquid phase) has been calibrated

in the present work as shown in Fig.6 with that of the work cited in the literature according to Deepak et al. (2012) as shown in Fig.5. According to fig.5 and fig.6 in both figure Velocity magnitude first increases length along the nozzle then the velocity is constant. It is clear that there is good agreement between the two models as regards to the velocity distribution.

4.1.2. The effect of inlet operating pressure on jet exit kinetic energy [Abrasive-garnet (63µm), volume fraction-10%]

The graph of variation of jet exit kinetic energy of the jet with inlet operating pressure has been calibrated in the present work as shown in Fig. 7 with that of the work cited in the reference literature according to Deepak et al. (2012) as shown in Fig. 6. From the (fig.6 and fig. 7) graphs a Jet exit kinetic energy is linearly proportional to corresponding inlet operating pressure,it is clear that there is good agreement between the two models as regards to the variation of jet exit kinetic.

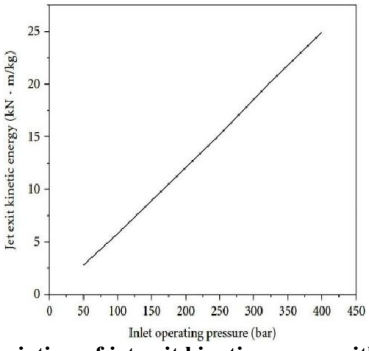

Fig. 6: variation of jet exit kinetic energy with inlet Operating pressure as given in reference [20].

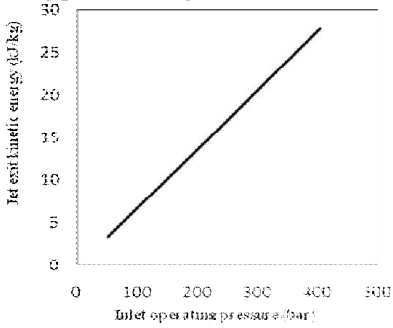

Fig. 7: Variation of Average exit kinetic energy of the jet with inlet operating pressure as per the present model.

4. 2 The effect of nozzle geometry, Abrasive size and Abrasives on skin friction coefficient at the wall and Jet exit kinetic energy (Inlet operating pressure: 40MPa, Abrasive: garnet, Abrasive size: 63µ, volume fraction: 10%)

The tested values of the parameters are given in Table 1, while varying a given parameters independently , all other were set to their typical values shown in Table 1 and inlet operating pressure 400 bar and volume fraction of abrasive is 10%. For geometrical analysis take the garnet abrasive and abrasive size is 63µm.

Table 1: Test parameters and values

Parameters	Value tested (mm)	Typical value (mm)
Nozzle Diameter	3.5, 3.8, 4, 4.1	4
Focus length	17, 17.5,18,18.2	17
Orifice diameter	1,1.3, 1.4, 1.5	1.3
Abrasive size	53, 60, 64, 65 (µm)	63µm
Abrasive	Aluminum oxide, Silicon carbide	Garnet

4.2.1 Effect of inlet diameter of nozzle on skin friction coefficient and jet exit kinetic energy

From Fig.8: the data plotted show that, the skin friction coefficient increases with increase in nozzle inlet diameter because from the particle erosion theory, erosion rate is directly proportional to function of impact angle (from equation 24) and when nozzle inlet diameter increases with also increase in impact angle and From Fig. 9 shows that the results obtained from analysis Jet exit kinetic energy increases with increase in nozzle inlet diameter because from the continuity equation Jet exit velocity is directly proportional to inlet diameter. The velocity of flow will increase with increase in nozzle inlet diameter hence jet exit kinetic energy will also increased.

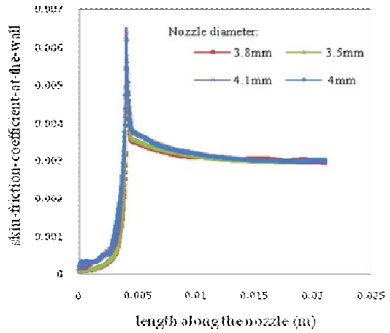

Fig. 8: Variation of skin friction coefficient at the wall of nozzle due to change of nozzle inlet diameter.

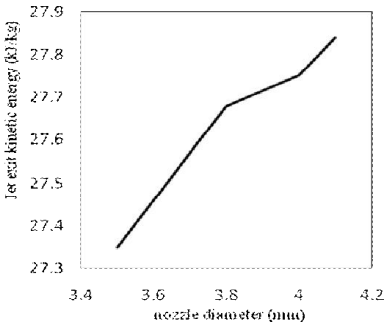

Fig. 9: Variation of jet exit kinetic energy due to change of nozzle inlet diameter.

4.2.2 Effect of Focus length of nozzle on Skin Friction Coefficient and Jet Exit Kinetic Energy

From Fig. 10 and Fig. 11 shows that the results obtained from analysis the skin friction coefficient slightly decreases and jet exit kinetic energy decreases with increase in focus length because according to Bernoulli's law the energy loss increases with increase in pipe length. According to Deepak et al [20] higher velocity of flow contribute to higher skin friction coefficient; hence the higher focus lengths have higher kinetic energy loss but slightly decreased skin friction coefficient at the wall of nozzle.

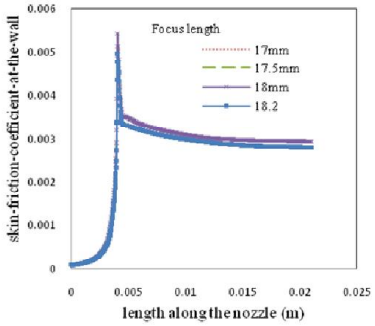

Fig. 10: Variation of skin friction coefficient at the wall of nozzle due to change of focus length.

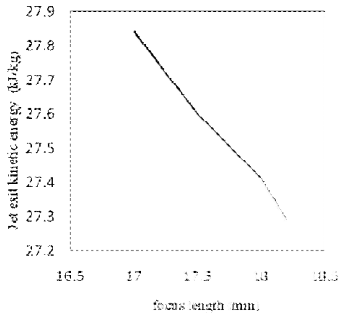

Fig. 11: Variation of jet exit kinetic energy due to Change of focus length.

4.2.3 Effect orifice diameter on Skin Friction Coefficient and Jet Exit Kinetic Energy

From Fig.12 the skin friction coefficient decreases with increase in orifice diameter because from the particle erosion theory, erosion rate is directly proportional to function of impact angle (from equation 24) and when orifice diameter increases with decrease in impact angle and From Fig. 13 shows that the Jet exit kinetic energy decreases with increase in orifice diameter because from the continuity equation jet exit velocity is inversely proportional to exit diameter. The velocity will decreases with increase in orifice diameter and from Fig.13 shows that the jet exit kinetic energy decreases with increase in orifice diameter.

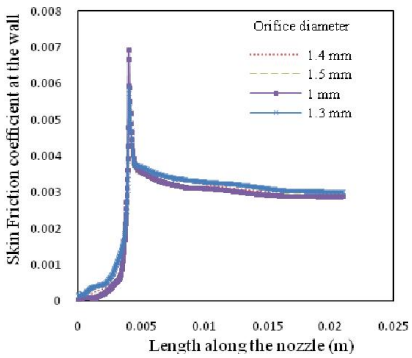

Fig. 12 : Variation of skin friction coefficient at the wall of nozzle due to change of orifice diameter.

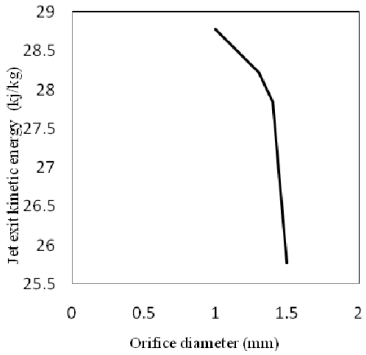

Fig. 13: Variation of jet exit kinetic energy due to change of orifice diameter.

4.2.4 Effect different abrasives on Skin Friction Coefficient and Jet Exit Kinetic Energy in single step nozzle

The maximum skin friction produced for different abrasive materials at same configuration take all other were set to their typical values shown in Table 2 and inlet operating pressure 40 bar and Abrasive type used garnet, aluminum oxide and silicon carbide and Abrasive size 63 µm shown in Fig.14 and jet exit kinetic energy shows in Fig. 15.

It is observed from the Fig. 14; the investigation is made on maximum skin friction produced by different abrasive particles namely garnet, aluminum oxide and silicon carbide on skin friction coefficient. It is seen from the Fig. 14 skin friction produced by garnet abrasive particle is highest and it is followed by aluminum oxide and silicon carbide abrasive particles. This trends is due to the effect of density of abrasive particles (silicon carbide ρ= 3170 kg/m^3, aluminum oxide ρ = 2719 kg/m^3 and garnet ρ = 2300 kg/m^3). Increase in the density of abrasive particles results in corresponding reduction velocity of the flow due to mass inertial effect and hence is reduction in skin friction coefficient.

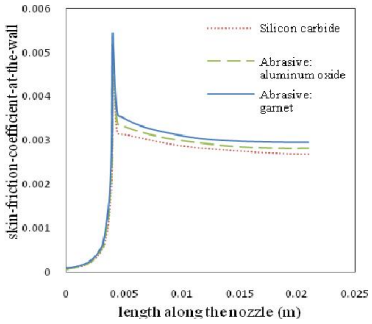

Fig.14: Variation of skin friction coefficient at the wall of nozzle due to change of abrasive

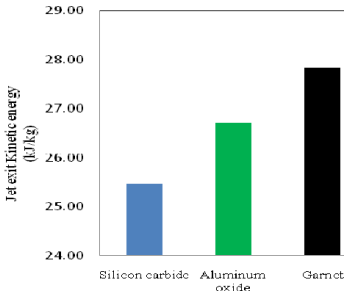

Fig. 15: Variation of jet exit kinetic energy due to change of abrasive

It is seen from the Fig. 15 that there is a marginal decrease in jet exit kinetic energy with increase in density of abrasive particles. As explained previously, density of abrasive particles in the fluid, higher is the fluid inertial resistance while transporting these abrasive particles leading to a reduction in exit velocity. Hence there is a corresponding decrease in jet exit kinetic energy with increase in abrasive particles. Jet exit kinetic energy produced by garnet abrasive particles is highest which is followed by aluminum oxide and silicon carbide abrasive respectively

4.2.5 Effect of Abrasive size on Skin Friction Coefficient and Jet Exit Kinetic Energy

From Fig. 16 shows that the results obtained from analysis for four different garnet abrasive sizes, which are only used once through and are not recalculated.

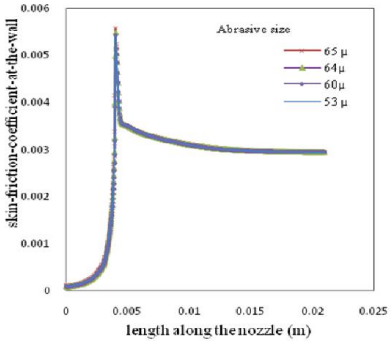

Fig. 16: Variation of skin friction coefficient at the wall of nozzle due to change of Abrasive size.

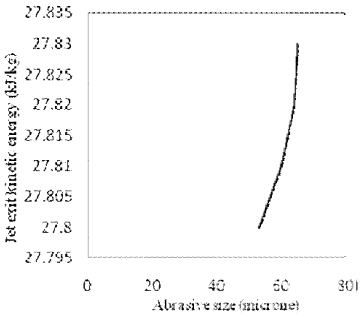

Fig. 17: Variation of jet exit kinetic energy due to change of Abrasive size.

Based on the Analysis at the critical section of nozzle an empirical formula developed for the Range of
P (Inlet Operating Pressure) – 100- 400 (bar)
D (Nozzle diameter) – 3.5 - 4.5 (mm)
d (orifice diameter) – 1 -1.5 (mm)
ρ (density of Abrasive Particle)–2300-3170 (kg/m^3)
L (focus length) – 17-18.2 (mm)

$$\text{Skin friction coefficient} = \frac{K\,(P)^{0.924}\,(D)^{0.428}}{(d)^{0.204}(\rho)^{0.342}\,(L)^{0.838}} \qquad (25)$$

Where K = 1.027x10^{-5} $= \frac{mm^2}{kgN}$

5. CONCLUSION

The following conclusions are drawn from the CFD simulation:

- Increase in nozzle inlet diameter results in significant increase in the skin friction coefficient and also increase in jet exit kinetic energy.
- Increase in focus length results in slightly decreases in the skin friction coefficient and also decrease in jet exit kinetic energy.
- Increase in orifice diameter results in significant decreases in the skin friction coefficient and also decrease in jet exit kinetic energy.
- Increased in abrasive particle density results in significant decreases in the skin friction coefficient and also decrease in jet exit kinetic energy.
- Increase in abrasive size results in slightly increase in the skin friction coefficient and also slightly increase in jet exit kinetic energy.

It is expected that higher wall shear stress will induce higher wear of the wall, and it is concluded from CFD analysis nozzle geometry is highly effect the wear rate and efficiency of AWSJ machining process. The simulation model can provide a lot of results to the user and it can be useful in studying the overall water suspension jet process and for the optimization of the nozzle geometry. In future analysis of multistep nozzle in AWSJ machining can be done with the help of CFD software package.

REFERENCES

1. N. C. Markatos, "Modelling of two-phase transient flow and combustion of granular propellants." *International Journal of Multiphase flow, vol. 12, no. 6, pp. 913-933, 1986.*
2. M. Hashish, Observation of wear of abrasive-waterjet nozzle materials, *Journal of Tribology* 116 (1994) 439-444.
3. Fluent User's Guide, vol. 3, Fluent Incorporated Publishers,Lebanon, 1998.
4. M. J. Steinkamp, T. T. Clark, and F. H. Harlow, "Twopointdescription of two-fluid turbulent mixing-II. Numericalsolutions and comparisons with experiments," *InternationalJournal of Multiphase Flow, vol. 25, no. 4, pp. 639–682, 1999.*
5. G. J. Brown, "Erosion prediction in slurry pipeline teejunctions," *Applied Mathematical Modelling, vol. 26, no. 2, pp. 155–170, 2002.*
6. Nanduri M, Taggart DG, Kim TJ (2002), The effects of system and geometric parameters on abrasive waterjet nozzle wear. *Int J Mach Tools Manuf* 42: 615-623.
7. J. Chahed, V. Roig, and L. Masbersnat, "Eulerian-eulerian two-fluid model for turbulent gas-liquid bubbly flows," *International Journal of Multiphase Flow*, vol. 29, no. 1, pp. 23–49, 2003.
8. U. Anand and J. Katz, "Prevention of nozzle wears abrasive water suspension jet (AWSJ) using porous lubricated nozzle, *"Journal of Tribology, vol.125, no.1, pp.168-180,2003.*
9. H. Liu, J. Wang, N. Kelson, R. Brown, A study of abrasive waterjet characteristics by CFD simulation, Journal of Materials Processing Technology 153-154 (2004) 488-493.
10. J. John RozarioJegaraj, N. Ramesh Babu, A strategy for efficient and quality cutting of material with abrasive waterjets considering the variation in orifice and focusing nozzle diameter, *Int. J. Mach. Tools Manuf.* 45 (12-13) (2005) 1443-1450.
11. K. Maniadaki, T. Kestis, N. Bilalis, A. Antoniadis, A finite element-based model for pure water-jet process simulation, *Int. J. Adv Manuf. Technol.* (2007) 31: 933-940.
12. B. S. Nie, J. Q. Meng, and Z. F. Ji, "Numerical simulationon flow field of pre-mixed abrasive water jet nozzle," in *Proceedingsof the Asia Simulation-7th International Conference on System Simulation and Scientific Computing (ICSC '08)*, pp.247–251, October 2008.
13. .. D. S. Srinivasu,N.RameshBabu, A neuro-geneticapproach for selection of process parameters in abrasive waterjet cutting considering variation in diameter of focusing nozzle, *in applied soft computing* 8 (2008) 809-819.
14. T. Nguyen, D.K. Shanmugam, and J. Wang, " Effect of liquid properties on the stability of an abrasive waterjet" *International Journal of Machine Tools and Manufacture, vol, 48, no. 10, pp.1138-1147, 2008.*
15. H.Z. Li, J. Wang, J.M. Fan, Analysis and modeling of particle velocities in micro-abrasive air jet, International Journals of Machine Tools & Manufacture 49 (2009) 850-858.
16. N. Pi and N. Q. Tuan, "A study on nozzle wear modeling in abrasive waterjet cutting," a*dvanced Materials Research*, vol.76, pp. 345–350, 2009.
17. M.G. Mostofa, K. Yong Kil, A. J. Hwan, computational fluid analysis of abrasive waterjet cutting head,*Journal of Mechanical Science and Technology* 24 (2010) 249-252.
18. M. Zohoor, S.HadiNourian, Development of an algorithm for optimum control process to compensate the nozzle wear effect in cutting the hard and tough material abrasive water jet cutting process,*Int. J AdvManufTechnol* (2012) 61:1019-1028.
19. Help documentation of 'GAMBIT 2.3.16' Software.
20. D. Deepak, D. Anjaiah D, K. VasuudevaKaranth, and N. Yagnesh Sharma, CFD Simulation of flow in an Abrasive Water Suspension Jet: The Effect of Inlet Operating Pressure and Volume Fraction on Skin Friction and Exit Kinetic Energy, *Hindawi Publishing Corporation, Advance in Mechanical Engineering, Volume* 2012*, Article ID* 186430.
21. Help documentation of 'Fluent 6.3.26' Software
22. S. Anwar, D. Axinte and A.A Becker, Finite element modelling of abrasive waterjet milled footprints Faculty of Engineering, Department of Mechanical, Materials and Manufacturing Engineering, University of Nottingham, NG7 2RD, UK, Volume 213, Issue 2, February 2013, Pages 180–193.

Note: This Paper/Article is scrutinised and reviewed by Scientific Committee, BITCON-2015, BIT, Durg, CG, India